Materials Research Bulletin 45 (2010) 705–709

Contents lists available at ScienceDirect

Materials Research Bulletin

journal homepage: www.elsevier.com/locate/matresbu

Multifunctional $Zn_{0.99-x}Mn_{0.01}Cu_xS$ nanowires: Structure, luminescence and magnetism

Jian Cao [a,b], Jinghai Yang [c,*], Yongjun Zhang [c], Lili Yang [c], Yaxin Wang [c], Dandan Wang [a,b], Ming Gao [c], Yang Liu [c], Xiaoyan Liu [c], Zhi Xie [d]

[a] Key Laboratory of Excited State Physics, Changchun Institute of Optics, Fine Mechanics and Physics, Chinese Academy of Sciences, 3888 Eastern Nan-Hu Road, Changchun 130033, PR China
[b] Graduate School of the Chinese Academy of Sciences, Beijing 100049, PR China
[c] Institute of Condensed State Physics, Jilin Normal University, No. 1301, Haifeng Street, Siping, Jilin Province 136000, PR China
[d] National Synchrotron Radiation Laboratory, University of Science and Technology of China, Hefei, Anhui 230029, PR China

ARTICLE INFO

Article history:
Received 22 August 2009
Received in revised form 13 January 2010
Accepted 18 February 2010
Available online 25 February 2010

Keywords:
A. Semiconductor
B. Chemical synthesis
C. XAFS
D. Luminescence
D. Magnetic properties

ABSTRACT

The wurtzite-type $Zn_{0.99-x}Mn_{0.01}Cu_xS$ ($x = 0$, 0.003, 0.01) nanowires were prepared by a simple hydrothermal method at 180 °C. The structure and morphology of the samples were characterized by X-ray diffraction (XRD), X-ray absorption fine structure (XAFS), transmission electron microscopy (TEM), high-resolution transmission electron microscopy (HRTEM), field emission scanning electron micrograph (FESEM) and X-ray photoelectron spectrum (XPS). The results showed that both the Mn^{2+} and Cu^{2+} ions substituted for the Zn^{2+} sites in the host ZnS. The ethylenediamine-mediated template was observed, which was used to explain the growth mechanism of the nanowires. The color-tunable emission can be obtained by adjusting the concentrations of Mn^{2+} and Cu^{2+} ions. The ferromagnetism was observed around room temperature.

1. Introduction

Developing multifunctional nanomaterials has attracted a great deal of attention in the past few years [1]. Dilute magnetic semiconductors (DMS) that allow the control of both the spin and charge of the carriers have been an active field of research for their interesting magnetic and luminescent properties, which can be used as effective platforms for biomedical imaging, drug delivery, protein separation and MRI contrast imaging [2–5]. ZnS based phosphors activated by transition metals are famous DMS materials with diverse properties, such as photoluminescence (PL), electroluminescence (EL) and magneto-optical properties. Recently, Park et al. [6] have tried to apply the ZnS:Mn, Cu and Cl phosphors for the EL device. The use of such phosphors has several excellent features, including spectral adjustable, high quantum efficiency and photostability. It is well known that $ZnS:Mn^{2+}$ nanomaterials usually exhibit a strong yellow-orange emission at about 580 nm [7], while $ZnS:Cu^{2+}$ nanomaterials show green and blue emission centered at 520 and 440 nm, respectively [8]. Therefore, color-tunable emission can be achieved by co-doping different concentrations of Mn^{2+} and Cu^{2+} ions into the ZnS lattice. As for the investigation of the magnetism for the ZnS based DMS nanomaterials, Kang et al. [9] have reported that the wurtzite-type $ZnS:Mn^{2+}$ nanowires synthesized by a chemical vapor transport method showed ferromagnetism around room temperature. Besides, few investigations were reported on the room temperature ferromagnetism for these materials.

In this paper, we synthesized the wurtzite $Zn_{0.99-x}Mn_{0.01}Cu_xS$ nanowires by the hydrothermal method. This method can be carried out at a relatively low temperature with quite cheap precursors of low toxicity, and the most important thing is that it is easier to incorporate the Mn^{2+} and Cu^{2+} ions into the ZnS host. In addition, we investigated the local structure surrounding the Mn^{2+} and Cu^{2+} ions, the possible growth mechanism, and the luminescent and magnetic properties of the samples.

2. Experimental

$Zn_{0.99-x}Mn_{0.01}Cu_xS$ ($x = 0$, 0.003, 0.01) nanowires were prepared by the hydrothermal technique. In our experiments, all chemicals were of analytical grade and were used as received without further purification. Firstly, $Zn(NO_3)_2{\cdot}6H_2O$, $Mn(NO_3)_2$

* Corresponding author. Tel.: +86 434 3290009; fax: +86 434 3294566.
E-mail address: jhyang1@jlnu.edu.cn (J. Yang).

0025-5408/$ – see front matter.
doi:10.1016/j.materresbull.2010.02.015

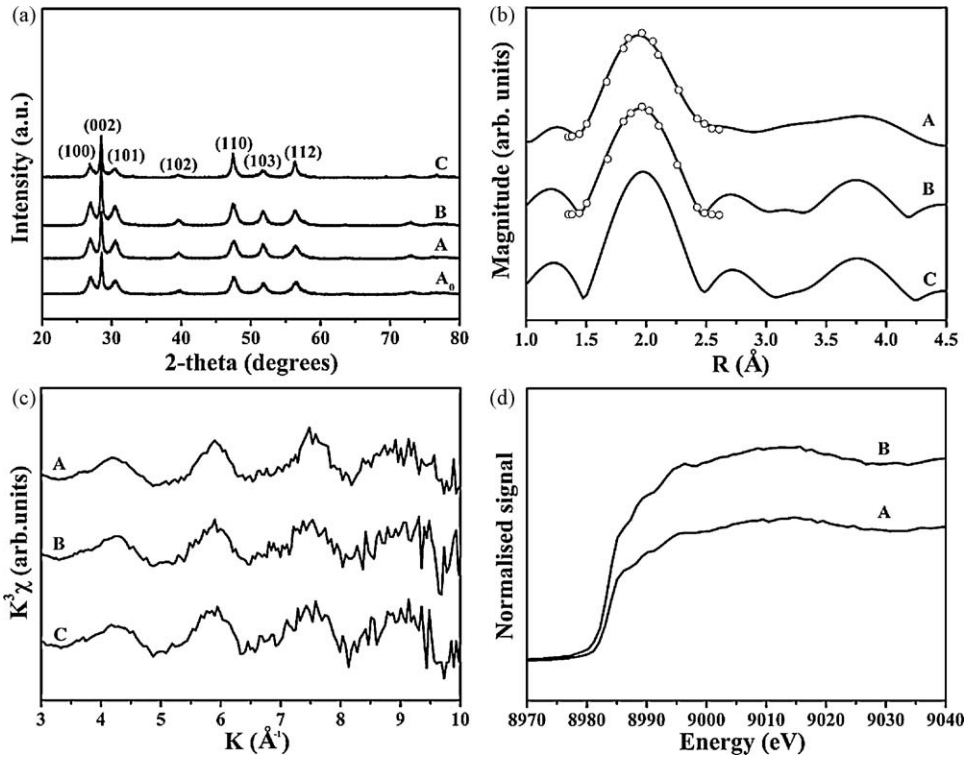

Fig. 1. (a) XRD patterns of (A_0) ZnS, (A) $Zn_{0.99}Mn_{0.01}S$, (B) $Zn_{0.987}Mn_{0.01}Cu_{0.003}S$ and (C) $Zn_{0.98}Mn_{0.01}Cu_{0.01}S$ nanowires. (b) *R*-space EXAFS patterns of Mn in (A) $Zn_{0.99}Mn_{0.01}S$, (B) $Zn_{0.987}Mn_{0.01}Cu_{0.003}S$ and (C) $Zn_{0.98}Mn_{0.01}Cu_{0.01}S$ nanowires. (c) EXAFS oscillation patterns measured at Mn *K*-edge for (A) $Zn_{0.99}Mn_{0.01}S$, (B) $Zn_{0.987}Mn_{0.01}Cu_{0.003}S$ and (C) $Zn_{0.98}Mn_{0.01}Cu_{0.01}S$ nanowires. (d) Cu *K*-edge XANES patterns for (A) $Zn_{0.987}Mn_{0.01}Cu_{0.003}S$ and (B) $Zn_{0.98}Mn_{0.01}Cu_{0.01}S$ nanowires.

and $Cu(NO_3)_2{\cdot}3H_2O$ were dissolved in 16 ml ethylenediamine (EN) and water (1:1 in volume ratio). The total amount of $Zn(NO_3)_2{\cdot}6H_2O$, $Mn(NO_3)_2$ and $Cu(NO_3)_2{\cdot}3H_2O$ was 0.5 mmol, the amount of $Mn(NO_3)_2$ was 0.01×0.5 mmol, the amount of $Cu(NO_3)_2{\cdot}3H_2O$ was $x \times 0.5$ mmol ($x = 0$, 0.003, 0.01). After stirring for 1 h, NH_2CSNH_2 (1.5 mmol) was put into the resulting complex. After stirring for 2 h, the colloid solution was transferred into a 20-ml Teflon-lined autoclave and kept at 180 °C for 12 h. After the reaction, the autoclave was taken out and cooled down to room temperature. The product was washed with ethanol and deionized water for several times and separated by centrifugation, and then dried at 80 °C for 1 h to get a white powder.

X-ray diffraction (XRD) pattern was collected on a MAC Science MXP-18 X-ray diffractometer using a Cu target radiation source. The Mn *K*-edge and Cu *K*-edge X-ray absorption fine structure (XAFS) measurements were performed at room temperature on beamline 1W1B at Beijing Synchrotron Radiation Facility, China. A double crystal Si (1 1 1) monochromator was used, and the signal was collected in fluorescence yield mode with a Lytle ion chamber detector. The data were collected in a mode of sample drain current under a vacuum better than 5×10^{-7} Torr. Transmission electron micrograph (TEM) was taken with a JEM-2100 electron microscope. The specimen was prepared by depositing a drop of the dilute solution of the sample in 2-propanol on a carbon-coated copper grid and drying at room temperature. Field emission scanning electron micrograph (FESEM) was taken with a FEI-XL30 electron microscope. EDAX microanalysis was performed at the FESEM magnification. X-ray photoelectron spectrum (XPS) was measured on an X-ray photoelectron spectroscopy (XPS) (VG ESCALAB Mark II). Photoluminescence (PL) measurement was carried out at room temperature, using 325 nm as the excitation wavelength, He–Cd laser as the source of excitation. Magnetic hysteresis loop was measured by a Lake Shore 7407 vibrating sample magnetometer (VSM) with the maximum field of 6 kOe.

3. Results and discussion

The XRD patterns of ZnS and $Zn_{0.99-x}Mn_{0.01}Cu_xS$ ($x = 0$, 0.003, 0.01) nanowires are shown in Fig. 1a. All the diffraction peaks can be well indexed as hexagonal wurtzite phase structure, which are consistent with the standard card (JCPDS No. 36-1450). Because the growth direction could be predicted by comparing the full width at half maximum (FWHM) of different XRD peaks [10]. Note that the (0 0 2) diffraction peak is stronger and narrower than the other peaks, suggesting a preferential growth direction along the *c*-axis. Within the sensitivity of XRD, we could not detect any secondary phases for the $Zn_{0.99-x}Mn_{0.01}Cu_xS$ nanowires. Fig. 1b shows the *R*-space extended XAFS (EXAFS) patterns of Mn in $Zn_{0.99-x}Mn_{0.01}Cu_xS$ ($x = 0$, 0.003, 0.01) nanowires. Because the amplitude and width of the peak at ~2 Å correspond to the number of nearest S neighbors around a Mn^{2+} ion and the Mn–S bond length, respectively. Using theoretical model supposed that the Mn^{2+} ions substituted for the Zn^{2+} sites, the back-Fourier transforms in the range 1.5–2.5 Å were calculated to separate the first shell oscillation. It can be seen that this structure model gives a good fitting quality, as displayed by the empty circles in Fig. 1b, suggesting that the Mn^{2+} ions are incorporated into the ZnS lattice substituting the Zn^{2+} sites. Fig. 1c shows the EXAFS oscillation patterns measured at Mn *K*-edge for $Zn_{0.99-x}Mn_{0.01}Cu_xS$ ($x = 0$, 0.003, 0.01) nanowires. It exhibits a quite similar oscillation shape for $Zn_{0.99-x}Mn_{0.01}Cu_xS$ ($x = 0$, 0.003, 0.01) nanowires, illustrating the essentially same local environment around the Mn^{2+} ions with no obvious concentration dependent variation. The normalized Cu *K*-edge near-edge XAFS (XANES) patterns for $Zn_{0.99-x}Mn_{0.01}Cu_xS$ ($x = 0.003$, 0.01) nanowires are shown in Fig. 1d, which are in good agreement with Ref. [11]. Based on the structure model assuming that the Cu^{2+} ions substituted for the Zn^{2+} sites, the Cu *K*-edge XANES patterns can be well reproduced by our calculations using FEFF8.2 [12]. Moreover, the pre-edge peak centered at 8985 eV is

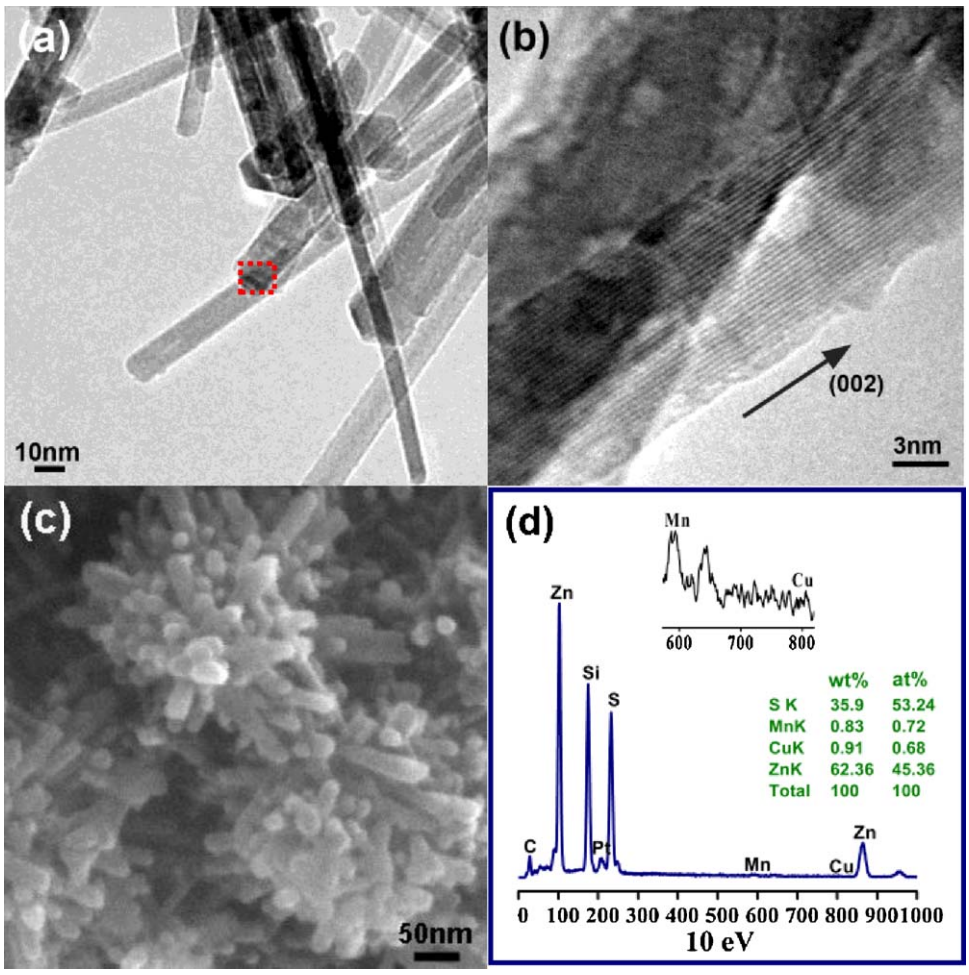

Fig. 2. (a) and (b) TEM and HRTEM images of $Zn_{0.99}Mn_{0.01}S$ nanowires. (c) FESEM image of $Zn_{0.98}Mn_{0.01}Cu_{0.01}S$ nanowires. (d) EDAX image of $Zn_{0.98}Mn_{0.01}Cu_{0.01}S$ nanowires, with the inset showing the enlarged image between 6 and 8 keV.

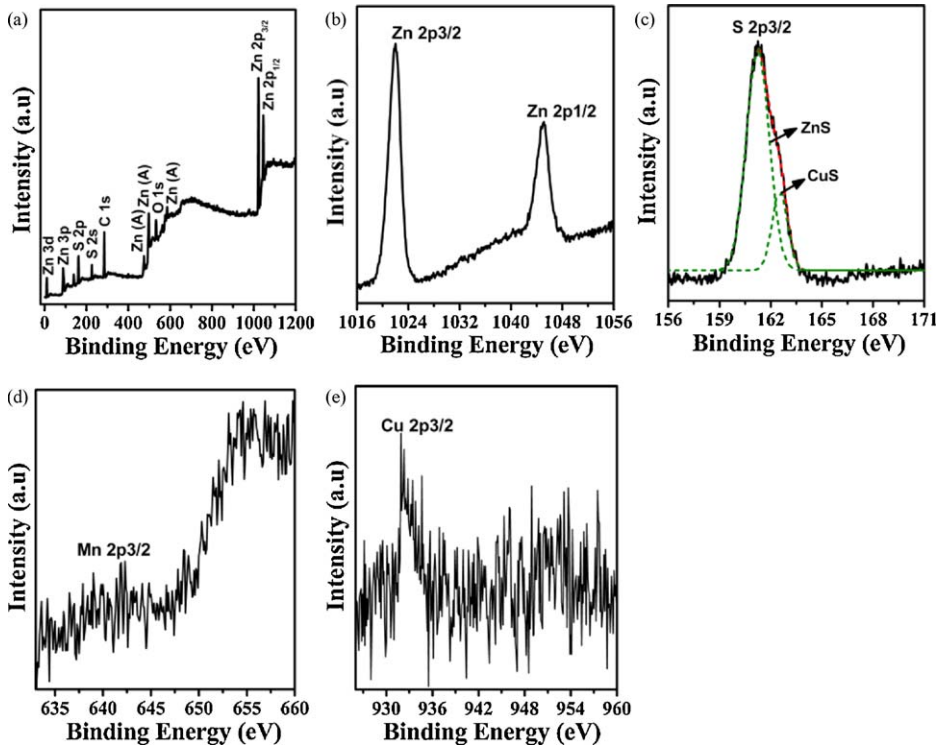

Fig. 3. XPS patterns of $Zn_{0.98}Mn_{0.01}Cu_{0.01}S$ nanowires: (a) survey spectrum and (b)–(e) high-resolution binding energy spectrum of Zn 2p, S 2p, Mn 2p and Cu 2p, respectively.

associated with the transitions from the *1s* states to the *3d* states. In principle, dipolar selection rules do not allow this excitation unless there is a strong hybridization between the *sp* hybrid orbital of ZnS and the *d* orbital of Cu^{2+} ions, which is only possible if the Cu^{2+} ions substitute for the Zn^{2+} sites in the host ZnS [13,14]. Consequently, both of the Mn^{2+} and Cu^{2+} ions are incorporated into the ZnS lattice substituting the Zn^{2+} sites.

The TEM image of $Zn_{0.99}Mn_{0.01}S$ nanowires (Fig. 2a) shows that the nanowires have a uniform diameter over their entire lengths and the average diameter is about 10 nm. The high-resolution TEM (HRTEM) image (Fig. 2b) of the single wire marked in Fig. 2a shows that the product grows along the (0 0 2) direction, which is well-oriented and good crystallization. The FESEM image of $Zn_{0.98}Mn_{0.01}Cu_{0.01}S$ nanowires shows some flowerlike structures built up by many nanowires with diameters of 20–30 nm (Fig. 2c), indicating the formation of the EN-mediated template [15]. Because EN is an important molecule precursor, which can react easily with Zn and S to form the $ZnS{\cdot}EN_{0.5}$ compound [16]. Consequently, the possible growth mechanism can be described as follows: firstly, thiourea released S^{2-} ions slowly with the aid of EN when the solution was sealed in the Teflon at the reaction temperature (180 °C) [17]; and then EN connected with Zn^{2+}, Mn^{2+}, Cu^{2+} and S^{2-} ions to form the $ZnMnCuS{\cdot}EN_{0.5}$ template. Under the hydrothermal condition, the $ZnMnCuS{\cdot}EN_{0.5}$ template dissociated from each other, eliminated the EN molecules from the $ZnMnCuS{\cdot}EN_{0.5}$ template. These detached wires would grow along the (0 0 2) direction because of the anisotropic crystallographic structure, in coincidence with the crystal growth habit [18]. The composition analysis of $Zn_{0.98}Mn_{0.01}Cu_{0.01}S$ nanowires by EDAX shown in Fig. 2d demonstrates that the sample contains Zn, S, Mn and Cu elements, and 0.72 at% Mn, 0.68 at% Cu can be detected (see inset of Fig. 2d).

Fig. 3 shows the XPS patterns of $Zn_{0.98}Mn_{0.01}Cu_{0.01}S$ nanowires, where Fig. 3a is the survey spectrum and Fig. 3b–e is the high-resolution binding energy spectrum for Zn 2p, S 2p, Mn 2p and Cu 2p, respectively. The presence of the carbon and oxygen in the survey spectrum (Fig. 3a) is due to the carbon tape used for the measurement and the adsorbed gaseous molecules such as O_2, CO_2 and H_2O, respectively [19]. In Fig. 3b–e, we can observe the Zn 2p3/2 peak at 1022 eV, the Zn 2p1/2 peak at 1045 eV [20], the S 2p3/2 peak at 161.25 eV [21] and 162.5 eV [22], the Mn 2p3/2 peak at 641.6 eV [23] and the Cu 2p3/2 peak at 932.5 eV [24], demonstrating that both of Mn and Cu exist in the form of +2 valance state (not 0 or +1).

The PL spectra of $Zn_{0.99-x}Mn_{0.01}Cu_xS$ ($x = 0$, 0.003, 0.01) nanowires are displayed in Fig. 4. The PL spectrum of the $Zn_{0.99}Mn_{0.01}S$ nanowires (red line) is composed of a strong yellow-orange emission centered at 586 nm and a very weak blue-green emission ranging from 400 to 540 nm, corresponding to the Mn^{2+} $4T^1$–$6A^1$ transition [25] and the defect related emissions [26], respectively. After adding Cu^{2+} ions into the $Zn_{0.99}Mn_{0.01}S$ nanowires, the intensity of the yellow-orange emission is reduced gradually, while the intensity of the green emission corresponding to the recombination from the shallow donor level (sulfur vacancy) to the t^2 level of Cu^{2+} [27] is increased as the Cu^{2+} doped-ratio increased (blue and green lines), illustrating that the energy absorbed by the ZnS host partly transferred to the Cu^{2+}-related luminescent centers [28]. Consequently, the color-tunable emission can be obtained by adjusting the concentrations of Mn^{2+} and Cu^{2+} ions.

Fig. 5 shows the magnetic hysteresis loop of $Zn_{0.98}Mn_{0.01}Cu_{0.01}S$ nanowires, which displays the ferromagnetism at room temperature. Because Cu is a kind of non-magnetic element, its secondary phases such as CuS displaying antiferromagnetism, Cu_2S showing no magnetism due to the fully filled *3d* orbitals, making the interpretation of ferromagnetism in $Zn_{0.98}Mn_{0.01}Cu_{0.01}S$ nanowires

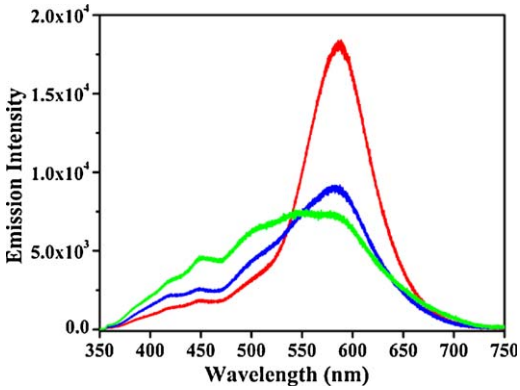

Fig. 4. PL spectra of $Zn_{0.99}Mn_{0.01}S$ (red line), $Zn_{0.987}Mn_{0.01}Cu_{0.003}S$ (blue line) and $Zn_{0.98}Mn_{0.01}Cu_{0.01}S$ (green line) nanowires. (For interpretation of the references to color in this figure legend, the reader is referred to the web version of this article.)

easier [29]. Generally, Anderson's super exchange (SE) [30] and Zener's double exchange (DE) [31] mechanism can be used to explain the magnetic coupling in many DMS compounds. One major difference between the two exchange mechanisms is the role of the mediator. In SE, the role of the mediator is played by a pair of *p* electrons of the host anions (S, Se and Te). One *p* electron is transferred to a neighboring transition metal ion, while the other directly exchange couples with another neighboring transition metal ion. This coupling normally reduces the kinetic energy and is ferromagnetism for the *d* shells that less than half full, and antiferromagnetism otherwise. The DE process is mediated by the conduction band of the host via a resonance state that mixes the same *d* orbitals of the transition metal ions and the extended conduction band states. Since Mn has no empty *d* orbital, the DE is prohibited [32]. Therefore the magnetism of the $Zn_{0.98}Mn_{0.01}Cu_{0.01}S$ nanowires is regulated by the SE. From the high-resolution binding energy spectrum of S 2p in Fig. 3c, the S 2p3/2 peak can be decomposed into two Gaussian peaks centered at 161.25 eV [21] and 162.5 eV [22], corresponding to the ZnS and CuS, respectively. Since the radius of Zn^{2+} and Cu^{2+} is so close, the bond length of the Cu–S and Zn–S is more or less the same. The slight variation of the coordination environments around the S^{2-} ions would affect the position of the binding energy of S 2p, leading to the existence of the two forms of S^{2-} ions. Hence, the SE process may occur between the two forms of S^{2-} ions, Mn^{2+} ions and Cu^{2+} ions. To clarify the mechanism of the ferromagnetism, much more theoretical work should be performed. In so doing, we have created

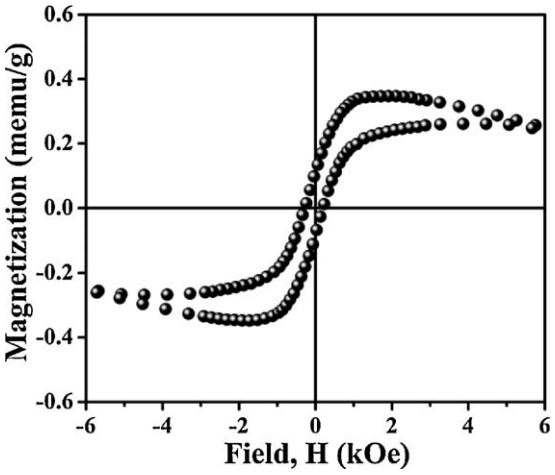

Fig. 5. Magnetic hysteresis loop of $Zn_{0.98}Mn_{0.01}Cu_{0.01}S$ nanowires.

multifunctional one-dimensional nanowires with exciting magneto-optical behavior, indicating its important applications for functional nanoscale devices.

4. Conclusions

In summary, we successfully synthesized $Zn_{0.99-x}Mn_{0.01}Cu_xS$ nanowires by a simple hydrothermal method. Both of the Mn^{2+} and Cu^{2+} ions substituted for the Zn^{2+} sites in the host ZnS. The samples showed a color-tunable emission by adjusting the concentrations of Mn^{2+} and Cu^{2+} ions. The room temperature ferromagnetism was observed, the mechanism of which can be explained by the super exchange mechanism.

Acknowledgments

The authors appreciate the financial support from the National Natural Science Foundation of China (Grant Nos. 60778040 and 60878039), National Programs for High Technology Research and Development of China (863) (Item No. 2009AA03Z303), Program for the development of Science and Technology of Jilin province (Item No. 20082112) and Cooperation Program between NSRL and BSRF.

References

[1] M. Li, Z. Chen, V.W. Yam, Y. Zu, ACS Nano 5 (2008) 905.
[2] S.A. Wolf, D.D. Awschalom, R.A. Buhrman, J.M. Daughton, S.V. Molnar, M.L. Roukes, A.Y. Chtchelkanova, D.M. Treger, Science 294 (2001) 1488.
[3] J.S. Kim, W.J. Rieter, K.M.L. Taylor, H. An, W. Lin, W. Lin, J. Am. Chem. Soc. 129 (2007) 8962.
[4] Y. Lin, S. Wu, Y. Hung, Y. Chou, C. Chang, M. Lin, C. Tsai, C. Mou, Chem. Mater. 18 (2006) 5170.
[5] S. Santra, H. Yang, P.H. Holloway, J.T. Stanley, R.A. Mericle, J. Am. Chem. Soc. 127 (2005) 1656.
[6] J.H. Park, S.H. Lee, J.S. Kim, A.K. Kwon, H.L. Park, S.D. Han, J. Lumin. 126 (2007) 566.
[7] B. Geng, L. Zhang, G. Wang, T. Xie, Y. Zhang, G. Meng, Appl. Phys. Lett. 84 (2004) 2157.
[8] W.Q. Yang, L. Daia, L.P. Youa, G.G. Qin, Phys. Lett. A 372 (2008) 4831.
[9] T. Kang, J. Sung, W. Shim, H. Moon, J. Cho, Y. Jo, W. Lee, B. Kim, J. Phys. Chem. C 113 (2009) 5352.
[10] S. Kar, S. Santra, H. Heinrich, J. Phys. Chem. C 112 (2008) 4036.
[11] R. Bogumil, P. Faller, P. Binz, Eur. J. Biochem. 255 (1998) 172.
[12] A.L. Ankudinov, B. Ravel, J.J. Rehr, S.D. Conradson, Phys. Rev. B 58 (1998) 7565.
[13] J. Cao, J. Yang, Y. Zhang, L. Yang, Y. Wang, M. Wei, Y. Liu, M. Gao, X. Liu, Z. Xie, J. Alloy Compd. 486 (2009) 890.
[14] J.P. Porres, A. Segura, J.F.S. Royo, J.A. Sans, J.P. Itié, A.M. Flank, P. Lagarde, A. Polian, Superlattice Microstruct. 42 (2007) 251.
[15] M.V. Limaye, S. Gokhale, S.A. Acharya, S.K. Kulkarni, Nanotechnology 19 (2008) 415602.
[16] F. Lu, W. Cai, Y. Zhang, Y. Li, F. Sun, J. Phys. Chem. C 111 (2007) 13385.
[17] Z. Zhao, F. Geng, H. Cong, J. Bai, H. Cheng, Nanotechnology 17 (2006) 4731.
[18] X. Chen, H. Xu, N. Xu, F. Zhao, W. Lin, G. Lin, Y. Fu, Z. Huang, H. Wang, M. Wu, Inorg. Chem. 42 (2003) 3100.
[19] S. Biswas, S. Kar, S. Santra, Y. Jompol, M. Arif, S.I. Khondaker, J. Phys. Chem. C 113 (2009) 3617.
[20] D.W. Langer, C.J. Vesely, Phys. Rev. B 2 (1970) 4885.
[21] X.R. Yu, F. Liu, Z.Y. Wang, Y. Chen, J. Electromagn. Spectrosc. Relat. Phemon. 50 (1990) 159.
[22] D. Brion, Appl. Surf. Sci. 2 (1980) 133.
[23] H.F. Franzen, M.X. Umana, J.R. McCreary, R.J. Thorn, J. Solid State Chem. 18 (1976) 363.
[24] D.L. Perry, J.A. Taylor, J. Mater. Sci. Lett. 5 (1986) 384.
[25] R.N. Bhargava, D. Gallagher, Phys. Rev. Lett. 72 (1994) 416.
[26] S. Biswas, S. Kar, S. Chaudhuri, J. Phys. Chem. B 109 (2005) 17526.
[27] W. Peng, G. Cong, S. Qu, Z. Wang, Opt. Mater. 29 (2006) 313.
[28] W. Wang, F. Huang, Y. Xia, A. Wang, J. Lumin. 128 (2008) 610.
[29] H.L. Liu, J.H. Yang, Y.J. Zhang, Y.X. Wang, M.B. Wei, D.D. Wang, L.Y. Zhao, J.H. Lang, M. Gao, J. Mater. Sci.: Mater. Electron. 20 (2009) 628.
[30] P.W. Anderson, Phys. Rev. 79 (1950) 350.
[31] C. Zener, Phys. Rev. 81 (1951) 440.
[32] I. Sarkar, M.K. Sanyal, S. Kar, S. Biswas, S. Banerjee, S. Chaudhuri, S. Takeyama, H. Mino, F. Komori, Phys. Rev. B 75 (2007) 224409.